

Supplementary Information for:

Sensitive and High Resolution Subcutaneous Fluorescence *in vivo* Imaging Using Upconversion Nanoparticles and Microarray

Xin Li, ‡^{a,b} Zhuoqi Li, ‡^{a,b} Wupeng Gan,^{a,b} Tongzhou Wang,^{a,b} Songmin Zhao,^{a,b} Ying Lu,^{a,b}

Jing Cheng^{a,b} and Guoliang Huang^{*a,b}

^a Department of Biomedical Engineering, Tsinghua University School of Medicine,

Beijing 100084, China. Fax: (86)-10-62797213; Tel: (86)-10-62797213;

E-mail: tshgl@tsinghua.edu.cn

^b National Engineering Research Center for Beijing Biochip Technology,

18 Life Science Parkway, Beijing 102206, China.

‡ These authors contributed equally to this work

FEM for upconverted photon propagation simulation

The upconverted photon propagation model in biological tissues can be described using the following coupled diffusion equations:

$$\begin{cases} \nabla \kappa_e(\mathbf{r}) \nabla \Phi_e(\mathbf{r}) - \mu_{ae}(\mathbf{r}) \Phi_e(\mathbf{r}) = -\mathbf{S}(\mathbf{r}) & (1.1) \\ \nabla \kappa_f(\mathbf{r}) \nabla \Phi_f(\mathbf{r}) - \mu_{af}(\mathbf{r}) \Phi_f(\mathbf{r}) = -\Phi_e^\gamma(\mathbf{r}) C \eta(\mathbf{r}) & (1.2) \end{cases} \quad (1)$$

where $\kappa_{e,f}(\mathbf{r})$ and $\mu_{ae,af}(\mathbf{r})$ stand for the diffusion and absorption coefficients, respectively, of excitation (subscript e) and emission light (subscript f); $\Phi_{e,f}(\mathbf{r})$ represents the intensities of excitation and fluorescence in tissue; $\mathbf{S}(\mathbf{r})$ and $\boldsymbol{\eta}(\mathbf{r})$ denote the distributions of excitation source and UNPs, respectively; C is a constant depicting the efficiency of the fluorophore; γ is a second constant related to the power dependence of the fluorophore. Different from the conventional fluorophore, for the UNPs used in this study, $\gamma=2$, determined experimentally to be quadratic in

Fig.1 (b). Robin-type boundary condition was then applied to solve these diffusion equations ¹.

Based on FEM ², $\Phi_{e,f}(\mathbf{r})$ can be solved using the weak-form equations Eq. (2), and by implementing the test function $\psi(\mathbf{r})$ as follows:

$$\left\{ \begin{array}{l} \int_{\Omega} (\kappa_e(\mathbf{r}) \nabla \Phi_e(\mathbf{r}) \nabla \psi(\mathbf{r}) + \mu_{ae}(\mathbf{r}) \Phi_e(\mathbf{r}) \psi(\mathbf{r})) d\mathbf{r} + \int_{\partial\Omega} \frac{1}{2q} \Phi_e(\mathbf{r}) \psi(\mathbf{r}) d\mathbf{r} \\ \qquad \qquad \qquad = \int_{\Omega} S(\mathbf{r}) \psi(\mathbf{r}) d\mathbf{r} \qquad (2.1) \\ \int_{\Omega} (\kappa_f(\mathbf{r}) \nabla \Phi_f(\mathbf{r}) \nabla \psi(\mathbf{r}) + \mu_{af}(\mathbf{r}) \Phi_f(\mathbf{r}) \psi(\mathbf{r})) d\mathbf{r} + \int_{\partial\Omega} \frac{1}{2q} \Phi_f(\mathbf{r}) \psi(\mathbf{r}) d\mathbf{r} \\ \qquad \qquad \qquad = \int_{\Omega} \Phi_e^2(\mathbf{r}) C\eta(\mathbf{r}) \psi(\mathbf{r}) d\mathbf{r} \qquad (2.2) \end{array} \right. , \quad (2)$$

Next, by discretizing the domain Ω and employing shape function $\mathbf{u}(\mathbf{r})$, Eq. (2) can be developed into the following set of linear matrix equations:

$$\left\{ \begin{array}{l} \mathbf{K}_e \cdot \Phi_e = \mathbf{M} \qquad (3.1) \\ \mathbf{K}_f \cdot \Phi_f = \mathbf{N} \cdot \mathbf{X} \qquad (3.2) \end{array} \right. , \quad (3)$$

where

$$\left\{ \begin{array}{l} K_{ei,ej} = \int_{\Omega} (\kappa_e(\mathbf{r}) \nabla u_i(\mathbf{r}) \cdot \nabla u_j(\mathbf{r}) + \mu_{ae}(\mathbf{r}) u_i(\mathbf{r}) u_j(\mathbf{r})) d\mathbf{r} + \frac{1}{2q} \int_{\partial\Omega} u_i(\mathbf{r}) u_j(\mathbf{r}) d\mathbf{r} \qquad (4.1) \\ M_{i,j} = \int_{\Omega} s(\mathbf{r}) u_j(\mathbf{r}) d\mathbf{r} \qquad (4.2) \end{array} \right. , \quad (4)$$

$$\left\{ \begin{array}{l} K_{fi,ij} = \int_{\Omega} (\kappa_f(\mathbf{r}) \nabla u_i(\mathbf{r}) \cdot \nabla u_j(\mathbf{r}) + \mu_{fe}(\mathbf{r}) u_i(\mathbf{r}) u_j(\mathbf{r})) d\mathbf{r} + \frac{1}{2q} \int_{\partial\Omega} u_i(\mathbf{r}) u_j(\mathbf{r}) d\mathbf{r} \qquad (5.1) \\ N_{i,j} = \int_{\Omega} \Phi_e^2(\mathbf{r}) u_i(\mathbf{r}) u_j(\mathbf{r}) d\mathbf{r} \qquad (5.2) \end{array} \right. . \quad (5)$$

In the above equations, $\Phi_{e,f}$ and \mathbf{X} denote the nodal values of $\Phi_{e,f}(\mathbf{r})$ and $C\eta(\mathbf{r})$, respectively, on the discretizing vertices. In the forward problem, as $\mathbf{K}_{e,f}$, \mathbf{M} and \mathbf{X} are known parameters that relate to the distribution of optical properties, excitation source and UNPs, respectively, the unknown fluorescence signal distribution can be obtained by solving Eq. (3).

Procedures for the preparation of sensitivity evaluation phantoms

Phantoms were prepared using epoxy resin (Araldite GY257, Laihe business Trading Co. Ltd, Tianjin, China), 20% intralipids (Kelun Pharmaceutical Co. Ltd, Sichuan, China), 1% diluted ink and solid paraffin as matrix, scattering, absorption and mould materials, respectively. The preparation procedures of sensitivity evaluation tissue phantoms are detailed as follows, which could be divided into two steps.

The first step was the preparation of the UNP cylinder inclusions in a series of concentrations. The solid paraffin was melted at 70°C and poured into a master mould containing cylindrical convex platforms. After the liquid paraffin was solidified, cylinder pits with 1.5 mm height and 3 mm diameter were formed on the surface of the paraffin. Next, phantom fluid with a total volume of 10 ml was prepared. According to the Van Staveren's Mie theory approximation³, the reduced scattering coefficient μ_s' of 10 % Intralipid is given by the following:

$$\mu_s = 2.54 \times 10^9 \times \lambda^{-2.4} \quad (1)$$

$$g = 1.1 - 0.58 \times 10^{-3} \lambda \quad (2)$$

$$\mu_s' = \mu_s (1 - g) \quad (3)$$

The reduced scattering coefficient $\mu_{s,20\% \text{ intralipid}}'$ of 20 % Intralipid can be calculated:

$$\mu_{s,20\% \text{ intralipid}}' = 2\mu_s' \quad (4)$$

The volume of the 20% intralipid could be calculated:

$$\mu_{s,20\% \text{ intralipid}}' \times V_{20\% \text{ intralipid}} = \mu_{s,Desired}' \times V_{total} \quad (5)$$

The 657 nm absorbance A of the 0.1% ink solution in 1 cm optical path was measured with the spectrophotometer (ND-1000, Thermo Scientific Inc.). In this study, $A = 2.17$. Then the absorbing coefficient of ink could be calculated:

$$\mu_{a,ink} = A \ln 10 \quad (6)$$

The absorption of water at 657 nm is very low⁴, as well as the epoxy resin, which can be ignored. The volume of 1% ink could be calculated:

$$\mu_{a,ink} \times V_{ink} = \mu_{a,Desired} \times V_{total} \quad (7)$$

Using the above equations, the required volumes of the 20% intralipid and 1% ink used in this study were calculated: $V_{20\% \text{ intralipid}} = 0.405$ ml and $V_{1\% \text{ ink}} = 0.06$ ml, to obtain the desired

phantom optical properties ($\mu_{sDesired}' = 10 \text{ cm}^{-1}$, $\mu_{aDesired} = 0.3 \text{ cm}^{-1}$) at the emission wavelength (657 nm).

The epoxy resin and the hardener (volume ratio: 10:4) were mixed with the intralipid, ink and various amounts of UNPs for 5 minutes to form different inclusions with a series of UNP concentrations (0.5, 0.2, 0.1, 0.05, 0.02, 0.01, 0.005 and 0.002 wt%). The phantom mixtures were put into the vacuum chamber to pump out the bubbles for about 20 minutes and then poured into the paraffin mould and vacuumed again for about 30 to 60 minutes. The full curing of UNP inclusions took approximately 24 hours at room temperature.

The second step was the preparation of tissue phantoms embedded with UNP inclusions and skin-like phantoms. The tissue phantom fluid was poured into an cuboid mould which contained the UNP solid inclusions at the bottom of the mould. The skin-like phantoms were prepared using a different set of optical property parameters [$\mu_a = 0.86 \text{ cm}^{-1}$ and $\mu_s' = 22.7 \text{ cm}^{-1}$ at the emission wavelength (657 nm)], and the skin-like phantom fluid was poured into a different mould with a thickness of 0.5 mm. Other preparation procedures for the tissue phantom and skin-like phantom are the same as that for the UNP inclusions. Finally, the skin-like phantoms were used to cover the tissue phantoms embedded with UNP inclusions.

Signal enhancement algorithm for subcutaneous microarray detection

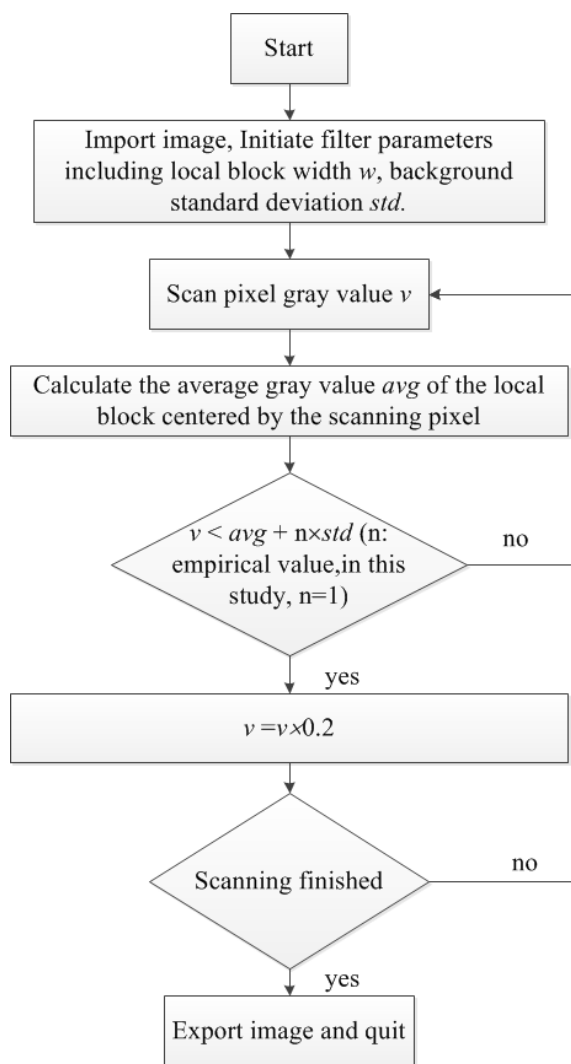


Figure S1. Flow chart of the algorithm

UNP quenching effect of OCA

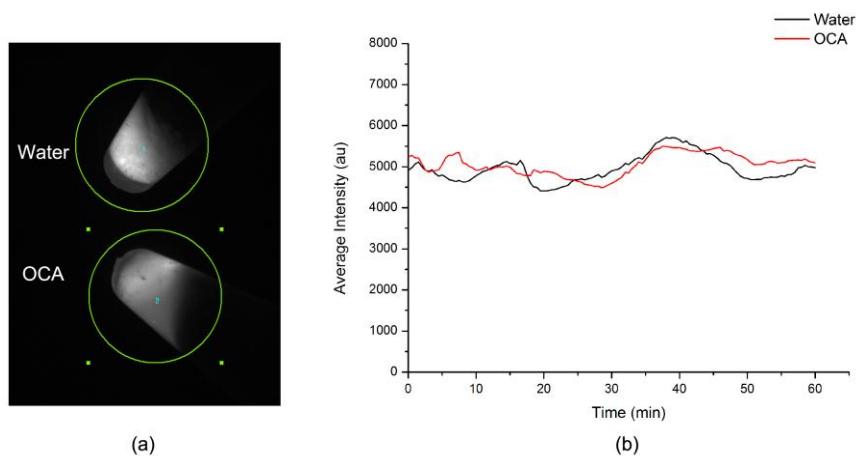


Figure S2. Real time fluorescence imaging of UNPs immersed in water and OCA for 1h. (a)

Fluorescence image of UNPs in water and OCA. (b) Average intensity statistics curve in the circle

areas in (a).

References

1. M. Schweiger, S. R. Arridge, M. Hiraoka and D. T. Delpy, *Med Phys*, 1995, **22**, 1779-1792.
2. S. RAO, *The Finite Element Method in Engineering*, Butterworth Heinemann London, 2004.
3. H. J. van Staveren, C. J. Moes, J. van Marie, S. A. Prahl and M. J. van Gemert, *Appl Opt*, 1991, **30**, 4507-4514.
4. R. M. Pope and E. S. Fry, *Appl Optics*, 1997, **36**, 8710-8723.